Biophysical *Journal*
Article

Biophysical Society

Reduced cardiac muscle power with low ATP simulating heart failure

Daniel A. Beard,[1] Bahador Marzban,[1] On Yeung Li,[2,3] Kenneth S. Campbell,[4] Paul M. L. Janssen,[5] Naomi C. Chesler,[6] and Anthony J. Baker[2,3,*]

[1]Department of Molecular and Integrative Physiology, University of Michigan, Ann Arbor, Michigan; [2]Veterans Affairs Medical Center, San Francisco, California; [3]Department of Medicine, University of California, San Francisco, California; [4]Department of Physiology and Division of Cardiovascular Medicine, University of Kentucky, Lexington, Kentucky; [5]Department of Physiology and Cell Biology, College of Medicine, The Ohio State University, Columbus, Ohio; and [6]Edwards Lifesciences Foundation Cardiovascular Innovation and Research Center and Department of Biomedical Engineering, University of California, Irvine, Irvine, California

ABSTRACT For patients with heart failure, myocardial ATP level can be reduced to one-half of that observed in healthy controls. This marked reduction (from ≈8 mM in healthy controls to as low as 3–4 mM in heart failure) has been suggested to contribute to impaired myocardial contraction and to the decreased pump function characteristic of heart failure. However, in vitro measures of maximum myofilament force generation, maximum shortening velocity, and the actomyosin ATPase activity show effective K_M values for MgATP ranging from ≈10 μM to 150 μM, well below the intracellular ATP level in heart failure. Thus, it is not clear that the fall of myocardial ATP observed in heart failure is sufficient to impair the function of the contractile proteins. Therefore, we tested the effect of low MgATP levels on myocardial contraction using demembranated cardiac muscle preparations that were exposed to MgATP levels typical of the range found in non-failing and failing hearts. Consistent with previous studies, we found that a 50% reduction in MgATP level (from 8 mM to 4 mM) did not reduce maximum force generation or maximum velocity of shortening. However, we found that a 50% reduction in MgATP level caused a 20%–25% reduction in maximal power generation (measured during muscle shortening against a load) and a 20% slowing of cross-bridge cycling kinetics. These results suggest that the decreased cellular ATP level occurring in heart failure contributes to the impaired pump function of the failing heart. Since the ATP-myosin ATPase dissociation constant is estimated to be submillimolar, these findings also suggest that MgATP concentration affects cross-bridge dynamics through a mechanism that is more complex than through the direct dependence of MgATP concentration on myosin ATPase activity. Finally, these studies suggest that therapies targeted to increase adenine nucleotide pool levels in cardiomyocytes might be beneficial for treating heart failure.

SIGNIFICANCE Cytoplasmic ATP levels are observed to be markedly reduced in the failing human heart and in the myocardium in animal models of heart failure compared with healthy control levels. We used an in vitro muscle-strip preparation in which the concentration of MgATP can be experimentally manipulated to investigate the hypothesis that the drop in MgATP observed in heart failure has a causal effect in reducing the capacity of the myocardium to generate mechanical power. We find that, while a reduction to 50% of normal MgATP concentration does not affect either maximal force generation or maximal velocity, this reduction does result in a significant reduction in maximal power generation, suggesting that the decreased level of ATP observed in heart failure impairs cardiac contraction power and contributes to impaired pump function.

INTRODUCTION

In heart failure, the intracellular ATP level may be reduced by ≈50% (1–3) relative to the non-failing heart where the intracellular ATP level is ≈8 mM (4–6). Similar reductions in myocardial ATP are observed commensurate with reductions in maximal cardiac power output in aging (7). The reduced level of ATP in heart failure has led to the intuitive suggestion that the failing heart is an "engine out of fuel" and that the decreased intracellular ATP level directly contributes to impaired cardiac contraction and heart failure (reviewed in (8)).

However, in vitro measurements of the effect of MgATP level on actomyosin ATPase activity and contraction reported

Submitted May 2, 2022, and accepted for publication July 22, 2022.

*Correspondence: anthony.baker@ucsf.edu

Editor: Michael Greenberg.

https://doi.org/10.1016/j.bpj.2022.07.029

an effective MgATP K_M of ≈150 μM for the actomyosin ATPase (9,10) and maximum shortening velocity of skeletal muscle fibers (10). Other studies found even lower MgATP K_M for the actomyosin ATPase of skeletal muscle fibers ($K_M = 20$ μM) (11) or cardiac muscle fibers ($K_M < 10$ μM) (12). Despite variability, these values are well below the millimolar range and suggest that the fall of ATP observed in heart failure may not be great enough to appreciably affect the contraction of cardiac myofilaments.

The goal of this study was to directly test whether the reduced level of ATP that is observed in heart failure affects myofilament contraction. We used permeabilized cardiac muscle fibers that were incubated with various levels of MgATP spanning the range observed in heart failure. In agreement with previous studies, we found that reductions in MgATP over the range 8 mM to 2 mM did not cause appreciable change in maximal force or shortening velocity. However, we found that a decreased MgATP level that mimicked heart failure caused reduced maximum contraction power generation. Prior computer simulations of the effects of phosphate metabolite levels on cross-bridge dynamics have revealed the role of increased inorganic phosphate concentration in impeding power generation in heart failure (5,13). However, in the current study a cross-bridge dynamics computational model did not capture the effect of low MgATP level to reduce maximum power generation. This finding suggests the existence of a novel mechanism connecting MgATP concentration and myocardial power generation that is not a simple reflection of the direct dependence of myosin ATPase activity on MgATP concentration.

In sum, our findings suggest that the decreased level of ATP observed in heart failure impairs cardiac contraction power and contributes to impaired pump function. Thus, therapies that increase the cellular MgATP level may be beneficial for treating heart failure.

MATERIALS AND METHODS

This institution is accredited by the American Association for the Accreditation of Laboratory Animal Care (Institutional PHS Assurance Number A3476-01). The study was approved by the Animal Care and Use Subcommittee of the San Francisco Veterans Affairs Medical Center and conformed to the Guide for the Care and Use of Laboratory Animals published by the National Institutes of Health (Revised 2011).

Preparation of demembranated cardiac trabeculae

Adult male C57BL/6J mice (Jackson Laboratory) were used ($n = 6$, age 11–14 weeks, mean body weight 28 g). Animals were deeply anesthetized with isoflurane 3%, and heparinized (100 U). Hearts were removed and immediately immersed in ice-cold arrest solution containing 120 mM NaCl, 30 mM KCl, and 0.1 mM $CaCl_2$; then perfused through the aorta with a modified Krebs-Henseleit solution containing 137 mM NaCl, 10 mM KCl, 1.2 mM $MgSO_4$, 1.2 mM NaH_2PO_4, 10 mM glucose, 20 mM $NaHCO_3$, 0.2 mM $CaCl_2$, and 30 mM 2,3,-butanedione monoxime. The perfusate was oxygenated with 95% O_2/5% CO_2 to give a pH of 7.4 at 22°C.

The right ventricular (RV) free wall was removed, and a piece of the wall near the tricuspid valve containing free-running trabeculae on the endocardial surface was dissected and pinned to a silicone platform. The number of trabeculae per heart varied (one from one animal, two from four animals, and three from one animal). Trabeculae were demembranated by immersion of the RV sample for 1 h in an ice-cold relaxing solution (see below) containing 2% Triton X-100 (Sigma-Aldrich). The RV sample was washed for 1 h in ice-cold relaxing solution and then transferred to a storage solution (1:1 mix of glycerol and relaxing solution). Samples were stored at −20°C and used within 2–16 days. There was no significant change over time for any of the measured parameters (data not shown).

Solutions

Previously, cytosolic MgATP level in non-failing rat heart was estimated to be ≈8 mM based on biochemical analysis, with correction for cytosolic water content and mitochondrial ATP fraction (4). In the current study, we used an activating solution containing 8 mM MgATP to represent the non-failing condition. To approximate the heart failure condition, where ATP level can drop by ≈50%, we used 4 mM MgATP and also tested 2 mM MgATP.

Muscles were first placed in relaxing solution containing 20 mM EGTA, 8, 4, or 2 mM MgATP, 12 mM creatine phosphate, and 100 mM *N*,*N*-bis[2-hydroxyethyl]2-aminoethane sulfonic acid; pH was adjusted to 7.1 with KOH and ionic strength adjusted to 200 mM with KCl (14). Muscles were briefly transitioned to preactivating solution in which calcium buffering was reduced by replacing 19.5 mM EGTA with HDTA (hexamethylenediamine-*N*,*N*,*NV*,*NV*-tetraacetate) (Fluka). Relaxing and preactivating solutions were both Ca^{2+}-free. Muscles were then placed in an activating solution containing 20 mM Ca^{2+}EGTA. The activating solution free [Ca^{2+}] was 30.9 μM (pCa 4.51). Measurements of contraction in this study used maximally calcium-activated contractions. The composition of solutions was determined using a computer program based on the methods of Fabiato and Fabiato (15). All solutions contained 1% (v/v) protease inhibitor cocktail P-8340 and 10 IU/mL creatine kinase (Sigma, St. Louis, MO).

Experimental arrangement

A demembranated trabecula was dissected and placed in relaxing solution in a small glass-bottomed chamber of a Permeabilized Fiber Test System (Model 1400A; Aurora Scientific, Aurora, ON, Canada) that was placed on an inverted microscope. The trabecula was attached with aluminum T-clips to a force transducer (Model 400; Aurora Scientific) and to a computer-controlled servo-motor.

Muscle sarcomeres were observed with a 40× objective, and sarcomere length was assessed with a video-based system (Model 900B; Aurora Scientific). In relaxing solution, muscle length was adjusted to set the sarcomere length to 2.0 μm, which is close to the diastolic sarcomere length observed in the beating mouse heart in vivo (16). All subsequent measurements of force and velocity were made at this baseline muscle length (Lo, sarcomere length = 2.0 μm).

Trabecula dimensions (length 784 ± 67 μm, width 137 ± 15 μm, thickness 97 ± 7 μm, $n = 12$) were measured. Muscle thickness was measured using a prism mounted next to the muscle. Measurements of muscle force were normalized to muscle cross-sectional area (estimated assuming an elliptical cross-section), and muscle shortening velocity was normalized to baseline muscle length (Lo).

Muscle activations

Experiments were performed in two groups (six trabeculae per group). Each trabecula was subjected to two contractions, one with 8 mM MgATP and one with low MgATP (either 4 mM or 2 mM). For all experiments, maximum force was reduced by 8% between activations. To minimize the effect of this

rundown, within each experimental group, for three trabeculae the first activation was 8 mM MgATP, and for the other three trabeculae the first activation was low MgATP (either 4 mM or 2 mM). This protocol allowed a paired comparison of 8 mM MgATP versus 4 mM MgATP ($n = 6$), and a paired comparison of 8 mM MgATP versus 2 mM MgATP ($n = 6$). In the pooled data, a total of 12 trabeculae were studied using 8 mM MgATP. For each group, one to two trabeculae per animal were studied. For each group, there was no interanimal difference among any of the measured parameters (ANOVA, not shown).

Force-velocity relationship

The relationship between contraction force and velocity was measured using isovelocity releases (17,18) as illustrated in Fig. 1 *A*. In brief, the length of the relaxed trabecula was increased by 10% (to 1.1 Lo). Following activation, a 2%–6% step decrease of muscle length caused a rapid drop of force. The length step was immediately followed by a ramp shortening at constant velocity, which resulted in muscle force equilibrating to the imposed shortening velocity.

The purpose of the step decrease of muscle length was to rapidly discharge the strained series elasticity and reduce the muscle force to a level that was close to the final force level achieved during the subsequent shortening ramp (17). Accordingly, a steady level of force was obtained during the shortening ramp as the muscle shortened to the initial length (Lo). As seen in Fig. 1 *A*, the faster shortening ramps were preceded by larger step decreases of muscle length in order to sufficiently reduce the force to the lower levels observed during rapid shortening.

The muscle force corresponding to a particular velocity was measured at the time that the muscle length passed through Lo. Following the step/ramp length protocol, the muscle was slackened with a rapid decrease of length to 0.8 Lo to determine the zero force level. Muscle length was then returned to 1.1 Lo over 20 ms. During a single activation lasting 12 s, multiple step/ramps were imposed in a non-sequential order that was the same for all experiments (velocities 6, 1, 3, 5, 0.5, 4, 2 muscle lengths per second). Following the last step/ramp, the muscle length was returned to Lo, and the isometric force was measured. Therefore, both the isometric force and the force-velocity data were obtained at the same muscle length (Lo).

The relationship between shortening velocity and the corresponding contraction force was fit to the Hill equation (19):

$$(P + a)(V + b) = (Po + a)b, \quad (1)$$

where P is the force during muscle shortening at velocity V, Po is the calculated peak isometric force, and a and b are constants with units of force and velocity respectively. The fit to the Hill equation was used to estimate the maximum power (where power is the product of force and velocity). Here, since force is reported per unit area (mN/mm^2, or kPa) and velocity is reported in units of muscle lengths per second, the product of these two quantities is power density, in units of W/L.

Rate constant of tension redevelopment (k_{tr})

Trabeculae were subjected to a length protocol to mechanically disrupt attached cross-bridges (Fig. 1 *B*). In brief, muscle length was rapidly reduced from Lo to 0.8 Lo for 10 ms. The slackened muscle underwent unloaded shortening. The muscle was briefly stretched to 1.05 Lo for 4 ms, after which muscle length was rapidly reset to Lo. This protocol reduced the muscle force to close to zero. The exponential rise of force after the length impulse was fitted to an exponential function (Fig. 1 *B*, *lower panel*) to obtain the rate constant of tension redevelopment (k_{tr}):

$$F = F_{max}[1 - \exp(-k_{tr}t)] + Fo, \quad (2)$$

where F, the force at time t after the length perturbation, rose from Fo just after the length perturbation to a final maximum of $F_{max} + Fo$. The values found for k_{tr} and V_{max} in this study are consistent with those recently reported for mouse trabeculae (20).

Statistical analysis

Curve-fitting of force-velocity data and k_{tr} data were performed using Prism 9 software (GraphPad Software, La Jolla, CA) and Microsoft Excel, respectively. Data are presented as mean ± SE. Statistical tests were performed using Prism 9 software with a significance level set at $p < 0.05$.

Simulation of muscle dynamics

The formulation and application of the computational model are detailed in Appendix A. This cross-bridge dynamics model was adapted from Marzban and Beard (21), which integrates elements of the model of Tewari et al. (5,22) with the myosin recruitment model of Campbell et al. (23). This

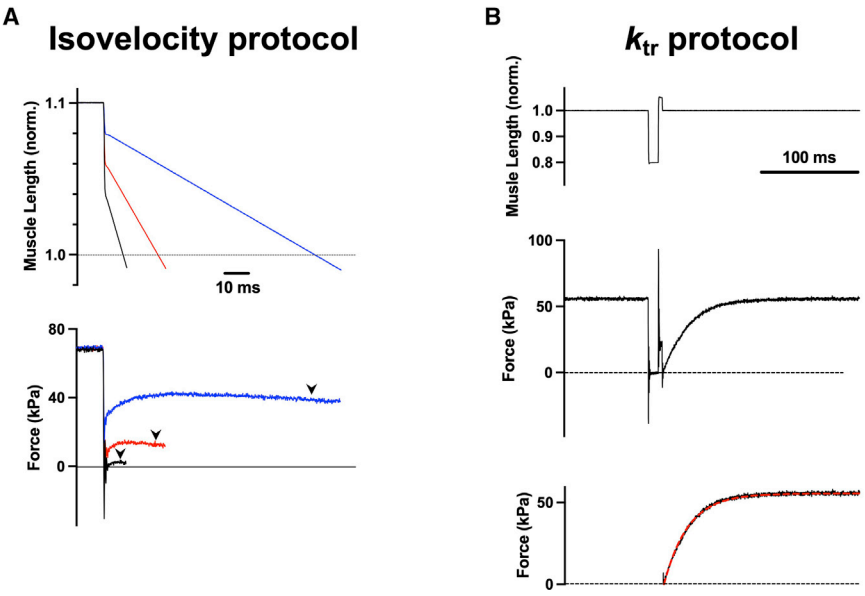

FIGURE 1 Mechanical protocols. (*A*) Measurement of force-velocity relation. Activated muscle with length set to 10% above the baseline length was rapidly shortened by 2%–6% (*upper panel*), which resulted in a rapid drop of force (*lower panel*). Muscle length was then shortened at constant velocity, and the corresponding muscle force was assessed when the muscle length shortened to the baseline length (*arrowheads* on force traces). (*B*) Measurement of the time constant of tension redevelopment (k_{tr}). Activated muscle at the baseline length (Lo) was rapidly shortened to 0.8 Lo for 20 ms, briefly stretched to 5% above Lo, and then reset to Lo (*upper panel*). This protocol reduced force to close zero (*middle panel*). Muscle force redeveloped exponentially with a time constant k_{tr} that was determined by fitting the data to Eq. 2 (*red trace in lower panel*).

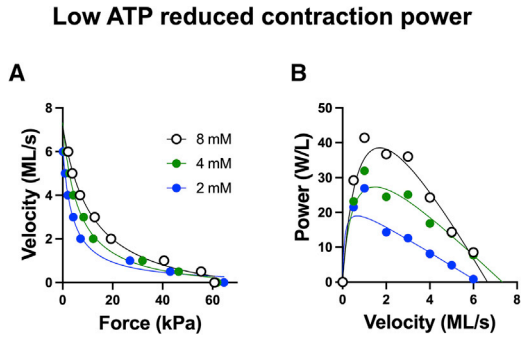

FIGURE 2 Representative example force-velocity data from individual trabeculae. (*A*) Shortening velocity versus muscle force measured during isovelocity contractions with MgATP levels set to 8 mM, 4 mM, or 2 mM. Lines show fits to the Hill equation. (*B*) The same data from (*A*) transformed to contraction power (force multiplied by velocity) versus shortening velocity. Lines are based on the fits shown in (*A*).

cross-bridge dynamics model was used to compare the model-predicted force-velocity relationship with the data from the skinned-fiber preparation.

RESULTS

Reduced MgATP caused reduced cardiac muscle power

Fig. 2 *A* shows representative examples of force-velocity relations for individual cardiac trabeculae in activating solutions containing 8 mM MgATP (typical of non-failing myocardium), or with MgATP reduced to 4 mM (typical of heart failure) or 2 mM. Lower MgATP levels were associated with a reduction in force at intermediate velocities. For all shortening velocities lower than maximal, lower MgATP resulted in lower force compared with contractions with 8 mM MgATP.

In contrast, Fig. 2 *A* shows that the estimated maximal velocities (obtained by extrapolating the observed force-velocity relationships to zero force) were not appreciably affected by MgATP concentration in the range assessed here. Moreover, the maximum level of force development measured at zero velocity was little affected by low MgATP level (see data summary in Table 1).

Fig. 2 *A* shows that the force-velocity data were closely fit to the Hill equation over most of the range. However, there was deviation between the data and fit at high force and low velocity. Similar to our data, previous studies of skeletal muscle have reported that the force-velocity data deviates from a hyperbola at the high-force, low-velocity end of the curve (24) (reviewed in (25)).

For low MgATP contractions, the lower force at each submaximal shortening velocity indicates reduced mechanical power (the product of force and velocity). Fig. 2 *B* shows a representative relationship between mechanical power and shortening velocity (same experiments as Fig. 2 *A*). Compared with 8 mM MgATP, mechanical power generation at intermediate shortening velocities was markedly reduced in low MgATP conditions compared with control 8 mM MgATP. Consistent with the deviation noted between the data and fit at the high-force, low-velocity end of the force-velocity curve, there was also a deviation between the data and fit at the low-velocity end of the power-velocity curve (Fig. 2 *B*). Despite uncertainty at the low-velocity end, there is a clear effect of low MgATP to depress both the force-velocity and power-velocity curves.

The effects of low MgATP are quantified for all experiments in Figs. 3, 4, 5, 6, and 7. Fig. 3 summarizes a paired analysis of the effect of low MgATP level on maximum power generation. For each experiment, maximum power was estimated from the fit of the force-velocity data to the Hill equation. In half of the experiments conducted to collect these data, MgATP level was changed from initially high (8 mM) to low (4 mM or 2 mM). For the other half, the order was swapped (low MgATP to high MgATP). Low MgATP level at both 4 mM and 2 mM significantly reduced maximum power compared with control. This effect did not depend on the order in which the high and low MgATP levels were presented. However, as evident from Fig. 3, the magnitude of the change in power level was greater when MgATP was decreased from 8 mM compared with when MgATP level was increased from either 4 mM or 2 mM. This asymmetry is likely due to deterioration (rundown) of the preparation that occurs between consecutive contractions, whereby the effect of rundown was superimposed on the ATP effect. Fig. 3 also shows that there was a statistically significant relationship between maximum power and MgATP level.

The reduced maximum power was associated with a greater curvature of the force-velocity relation at low compared with control MgATP level, as evident in Fig. 2 *A*. This effect of

TABLE 1 Mechanical properties of myocardium measured with 8 mM MgATP versus 4 mM MgATP, and with 8 mM MgATP versus 2 mM MgATP

	8 mM vs. 4 mM MgATP			8 mM vs. 2 mM MgATP		
	8 mM	4 mM	*p*	8 mM	2 mM	*p*
Max. force (kPa)	60.7 ± 5.3	63.6 ± 3.9	NS	52.1 ± 3.1	61.3 ± 2.3	0.03
Max. velocity (Lo/s)	7.13 ± 0.47	6.47 ± 0.70	NS	7.71 ± 0.70	6.89 ± 0.54	NS
a/Po	0.15 ± 0.02	0.09 ± 0.02	<0.01	0.13 ± 0.01	0.02 ± 0.01	<0.01
Max. power (W/L)	38.3 ± 3.2	29.9 ± 1.8	0.015	34.9 ± 1.6	23.5 ± 2.8	<0.01
Norm. power (s^{-1})	0.63 ± 0.01	0.47 ± 0.02	<0.0001	0.67 ± 0.03	0.38 ± 0.04	<0.0001
k_{tr} (s^{-1})	34.9 ± 1.0	28.1 ± 1.3	0.011	40.7 ± 3.5	25.8 ± 2.0	<0.01

Values are means ± SE, n = 6/group. NS, not significant.

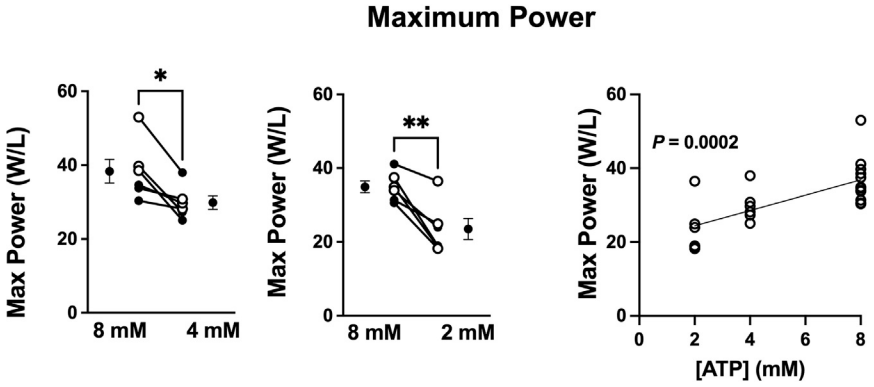

FIGURE 3 Low MgATP reduced contraction power. Maximum power (W/L) was significantly reduced by low MgATP level in paired experiments comparing 8 mM with 4 mM (*left panel*) or 8 mM with 2 mM (*middle panel*). Values in each pair are connected by a line, and for each pair the first measured condition is indicated by an open symbol (*$p < 0.05$, **$p < 0.01$, paired *t*-test). The mean value per group (± SE, n = 6) at each ATP level is also shown. For all experiments (*right panel*), there was a significant relationship between contraction power and MgATP level.

MgATP level on the curvature of the force-velocity relation is quantitated in Fig. 4 from the composite parameter a/Po of Eq. 1, where lower values indicate greater curvature (see materials and methods). There was a statistically significant relationship between a/Po and MgATP level. Although the physiological interpretation of a/Po remains uncertain, when comparing force-velocity curves with similar maximum velocity and maximum force levels, a greater curvature (lower a/Po) will be associated with lower maximal power. In this study, low MgATP level did not appreciably affect maximum velocity or maximum force. Thus, the lower a/Po observed with low MgATP level is consistent with the effect of low MgATP to reduce maximum power. Despite some uncertainty in the estimation of maximum power due to divergence between the force-velocity data and fitted values at low shortening velocities, the effect of low MgATP to reduce maximum power was supported by the observed effect of low MgATP to reduce a/Po.

Figs. 5 and 6 illustrate that there was no appreciable effect of MgATP level on maximal velocity or on maximal force in these experiments. Fig. 5 summarizes the effects of low MgATP on maximum shortening velocity (the velocity calculated at zero load from the Hill equation). The small differences in the maximum shortening velocity observed between MgATP levels of 8 mM and 4 mM and between 8 mM and 2 mM were not statistically significant. Similarly, Fig. 6 shows that there was not a significant change in maximum force development at zero velocity (experimentally measured isometric force) when comparing 8 mM MgATP with 4 mM MgATP. However, there was a significant increase in maximum force when comparing 8 mM MgATP (maximal force of 52.1 ± 3.1 kPa) with 2 mM MgATP (maximum force of 61.3 ± 2.3 kPa) ($p < 0.05$, $n = 6$/group).

Cross-bridge cycling kinetics was assessed by estimating the apparent rate constant of tension redevelopment (k_{tr}) after mechanical disruption of cross-bridges. Fig. 7 *A* shows exemplar tension-redevelopment curves at the three MgATP levels, showing that reducing MgATP slowed the rate of tension redevelopment (decreased k_{tr}). Estimates of k_{tr} are summarized in Fig. 7 *B*, illustrating that there were significant differences in k_{tr} when comparing 8 mM with both 4 mM MgATP and 2 mM MgATP, and a significant relationship between k_{tr} and ATP level.

For all experiments, Fig. 8 *A* summarizes the effects of low MgATP level on the force-velocity relation and the reduced contraction power observed at low MgATP. Moreover, the relationship between power generation and the rate of tension development is explored in Fig. 8 *B* by plotting maximum power generation versus k_{tr}. Analyzing data from all three MgATP levels in a composite data set, the relationship between maximum power and k_{tr} shows a

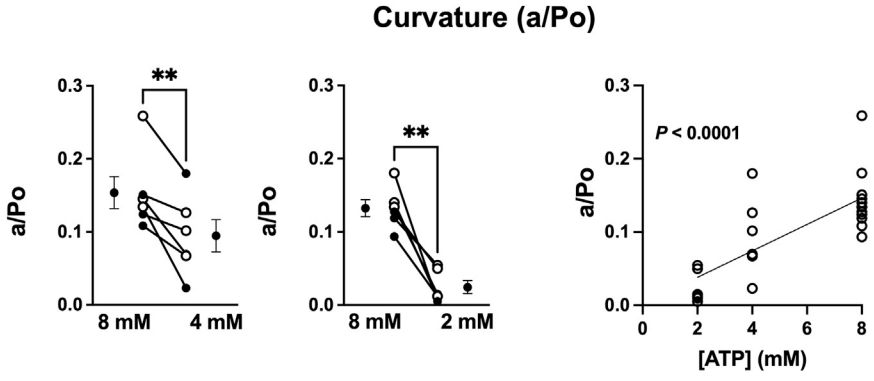

FIGURE 4 Low MgATP increased the curvature of the force-velocity relation. Low MgATP resulted in greater curvature of the force-velocity relation (lower values of a/Po) in paired experiments comparing 8 mM with 4 mM (*left panel*) or 8 mM with 2 mM (middle panel) (**$p < 0.01$, paired *t*-test). The mean value per group (± SE, n = 6) at each ATP level is also shown. For all experiments (*right panel*), there was a significant relationship between a/Po and MgATP level.

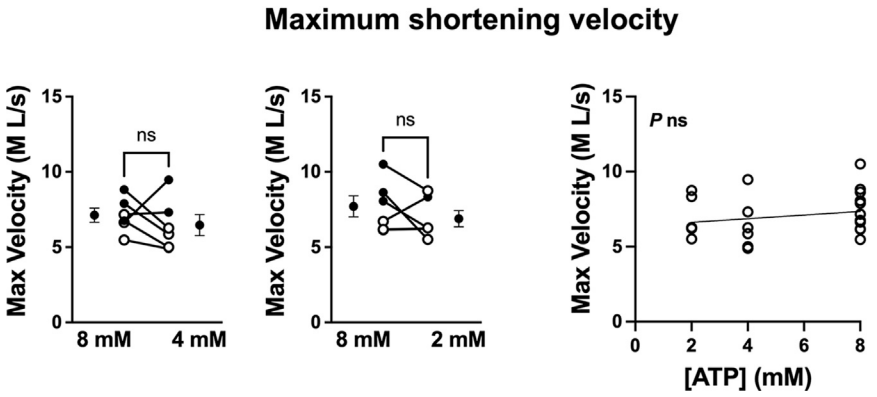

FIGURE 5 Low MgATP did not reduce maximum shortening velocity. Maximum shortening velocity (muscle lengths s^{-1}) was unchanged by low MgATP level in paired experiments comparing 8 mM with 4 mM (*left panel*) or 8 mM with 2 mM (*middle panel*). The mean value per group (± SE, n = 6) at each ATP level is also shown. For all experiments (*right panel*), there was no significant relationship between maximum shortening velocity and MgATP level.

correlation coefficient of $r = 0.55$ with a statistical significance indicated by $p < 0.01$.

Computer modeling of muscle dynamics

Fig. 9 shows a comparison of predictions of the cross-bridge dynamics model (see Appendix A) to the force-velocity data from Fig. 8. The solid lines in Fig. 9 represent the best fit of the data obtained at the three MgATP concentrations, illustrating that, regardless of adjustments made to the adjustable parameter values, the model does not reproduce the observed dependence of the force-velocity curve or the tension development kinetics on [MgATP]. Parameter values associated with these simulations are listed in Table 2. The model, in the form applied here, invokes a value of $K_{MgATP} = 0.50$ mM for the myosin ATPase-MgATP dissociation constant. This value, estimated by Tewari et al. (22), is consistent with MgATP binding to myosin ATPase being relatively insensitive to the MgATP concentration over the range of values studied here. As a result, the model behavior is relatively insensitive to [MgATP]. Yet, even allowing the parameter K_{MgATP} to attain arbitrarily high values (results not shown), the model is not able to capture the observed dependence of intermediate levels of force and velocity on [MgATP], indicating that the mechanism responsible for the observed behavior is not captured in the model.

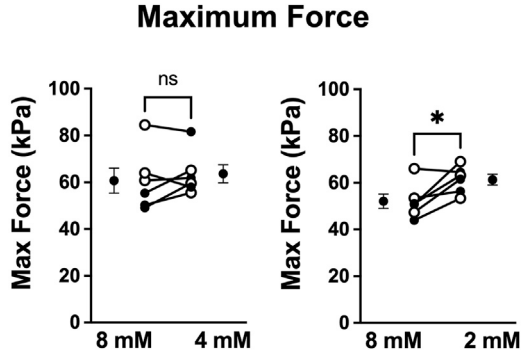

FIGURE 6 Effect of low MgATP on maximum force. Maximum force developed per muscle area (stress, kPa) was unchanged in paired experiments comparing 8 mM with 4 mM MgATP (*left panel*) but increased in paired experiments comparing 8 mM with 2 mM MgATP (*right panel*) (*$p < 0.05$, paired *t*-test). The mean value per group (± SE, n = 6) at each ATP level is also shown.

DISCUSSION

The major finding of this study is that a 50% decrease of MgATP concentration from 8 mM to 4 mM results in biologically substantial and statistically significant decreases in maximum contraction power and rate of tension

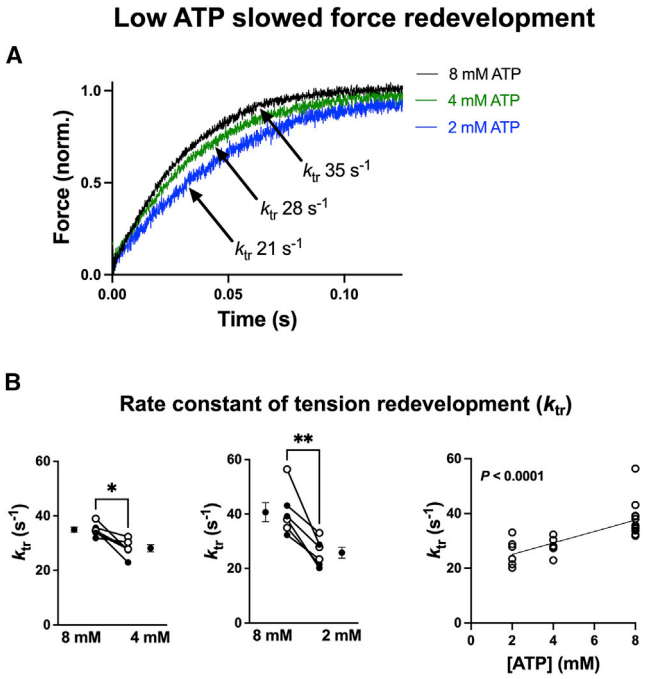

FIGURE 7 Low MgATP slowed force development kinetics. (*A*) Example traces of tension redevelopment after mechanical disruption of cross-bridges. Low MgATP level slowed the time course of tension redevelopment (decreased the rate constant of tension redevelopment, k_{tr}). (*B*) k_{tr} was significantly reduced by low MgATP level in paired experiments comparing 8 mM with 4 mM (*left panel*) or 8 mM with 2 mM (*middle panel*) (*$p < 0.05$, **$p < 0.01$, paired *t*-test). The mean value per group (± SE, n = 6) at each ATP level is also shown. For all experiments (*right panel*), there was a significant relationship between k_{tr} and MgATP level.

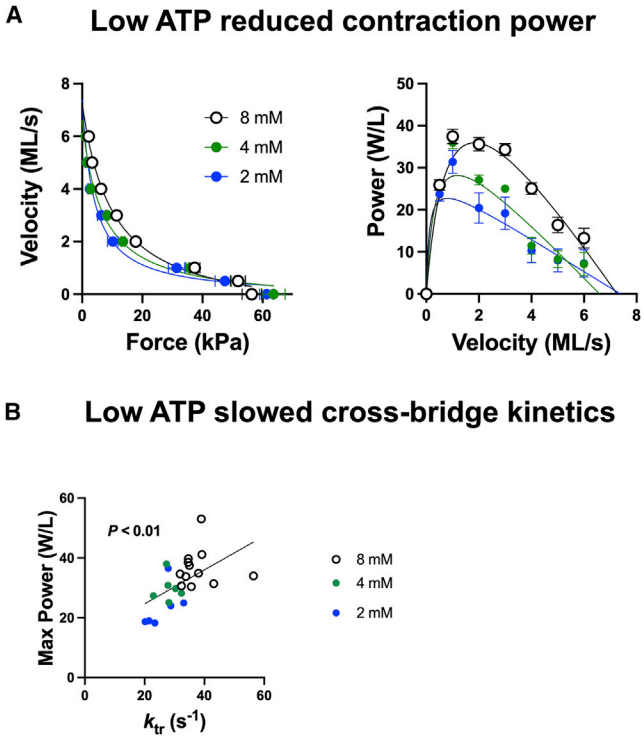

FIGURE 8 Pooled data for all experiments. (*A*) Low MgATP reduced contraction power. For all experiments, shortening velocity versus muscle force was measured during isovelocity contractions with MgATP levels set to 8 mM (n = 12), 4 mM (n = 6), or 2 mM (6) (*left panel*). Lines show fits to the Hill equation. Right panel shows the same data transformed to contraction power (force multiplied by velocity) versus shortening velocity. Lines are based on the fits shown in the left panel. Error bars indicate SE (when the SE exceeds the symbol size). (*B*) Low MgATP slowed cross-bridge kinetics. Low MgATP level reduced both maximum power and k_{tr}. There was a significant relationship between maximum power and k_{tr}.

development in mouse cardiac trabeculae in vitro. These findings are significant because in heart failure the intracellular ATP level is decreased over a similar range. Thus, decreased ATP level in heart failure could directly contribute to myofilament dysfunction, impaired tension development kinetics, reduced power output, and decreased pump function, consistent with the description of the failing heart as an "engine out of fuel" (8).

Decreased MgATP as a causal mechanism in heart failure

In heart failure, intracellular ATP level may be decreased due to a variety of mechanisms including mitochondrial dysfunction and depletion of the adenine nucleotide pool (6). Since the free energy of MgATP hydrolysis represents the driving force for mechanical power generation in muscle, it is reasonable to expect a relationship between mechanical function and MgATP level. However, even in heart failure the ATP level remains within the millimolar range and well above the apparent K_M for the actomyosin ATPase and maximum shortening velocity ($\approx$10–150 μM) (9–12). The high affinity of actomyosin for MgATP implies that the intracellular MgATP level would not be limiting in pathological states where the MgATP level is reduced yet remains in the millimolar range (26). The present data agree with these prior observations on the effects of [MgATP] on maximal force and shortening velocity, yet suggest that cardiac muscle dynamics at intermediate forces and velocities are indeed sensitive to changes in [MgATP] over the 4- to 8-mM range. This unexpected result suggests that reductions in ATP level observed in heart failure may be functionally important.

In agreement with the in vitro studies of Cooke and Bialek (10), we find that the maximum shortening velocity was not limited by MgATP level in the millimolar range. Moreover, we find that maximum force development was also not limited by MgATP level, and even increased slightly when MgATP was reduced from 8 mM to 2 mM, a finding that is also consistent with the observations of Cooke and Bialek in skeletal muscle (10) and Ebus et al. in cardiac muscle (12). Maximum force is thought to increase with decreasing [MgATP] because MgATP association is necessary for cross-bridge detachment. As a result, in the isometric state the population of attached cross-bridges at 2 mM [MgATP] is greater than at 8 mM [MgATP]. However, reducing [MgATP] has the opposite

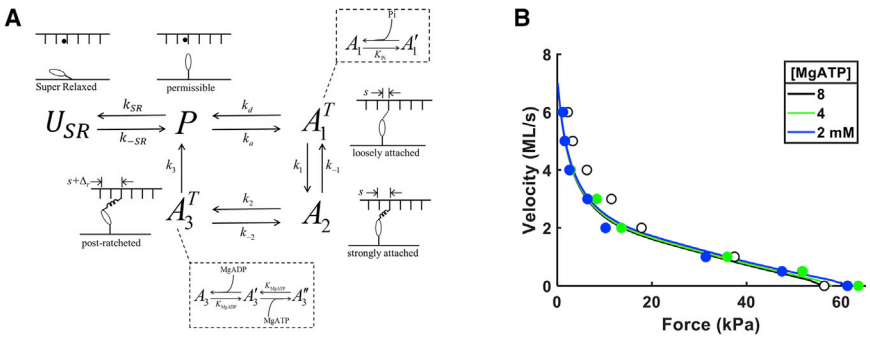

FIGURE 9 Simulation of muscle dynamics. (*A*) Schematic of cross-bridge dynamics model. This model was adapted from Marzban and Beard (21), which integrates elements of the model of Tewari et al. (5,22) with the model of transition between super-relaxed (SRX) and non-super-relaxed (non-SRX) states of Campbell et al. (23). The state U_{SR} represents myosin heads in the SRX state. The variable P represents the proportion of myosin heads that are in the permissive states (adjacent to calcium-activated myosin-binding site). The states A_1, A_2, and A_3 represent loosely bound, strongly bound (pre-ratcheted), and post-ratcheted states. For skinned-fiber simulations considered here we assume saturating calcium conditions, and thus no non-permissive (non-calcium bound) state is included in the model formulation. (*B*) Fit of steady-state model predictions of force versus sliding velocity to data obtained at [MgATP] = 8, 4, and 2 mM.

TABLE 2 Estimated model parameters

Parameter description	Symbol	Value	Unit	Source
Myosin-actin rate of attachment	k_a	373	s^{-1}	fit to data in Fig. 9
Myosin-actin rate of unattachment	k_d	103	s^{-1}	fit to data in Fig. 9
Weakly bound to strongly bound transition rate	k_1	40.1	s^{-1}	fit to data in Fig. 9
Strongly bound to weakly bound transition rate	k_{-1}	17.1	s^{-1}	fit to data in Fig. 9
Ratcheting transition rate	k_2	419	s^{-1}	fit to data in Fig. 9
Ratcheting reverse transition rate	k_{-2}	2.79	s^{-1}	fit to data in Fig. 9
Myosin-actin rate of detachment	k_3	44.3	s^{-1}	fit to data in Fig. 9
[Pi] dissociation constant	K_{Pi}	4.007	mM	(22)
[MgADP] dissociation constant	K_{MgADP}	0.194	mM	(22)
[MgATP] dissociation constant	K_{MgATP}	0.50	mM	(22)
Strain-dependency parameter	α_1	15.14	μm^{-1}	(22)
Strain-dependency parameter	α_2	10.06	μm^{-1}	(22)
Strain-dependency parameter	α_3	277	μm^{-2}	fit to data in Fig. 9
Strain-dependency parameter	s_3	0.00994	μm	(22)
Rate of transition to SRX state	k_{SR}	9.09	s^{-1}	fit to data in Fig. 9
Rate of transition to non-SRX state	k_{-SR}	250	s^{-1}	[a]
SRX transition force-dependency parameter	σ_0	33.1	kPa	fit to data in Fig. 9
Stiffness constant	$k_{stiff,1}$	1393	kPa	fit to data in Fig. 9
Post-ratchet stiffness constant	$k_{stiff,2} \times \Delta r$	133	kPa	fit to data in Fig. 9

[a]Arbitrary value.

effect on myofilament sliding velocity. This is because in the low MgATP limit, the inhibition of detachment is associated with a rigor-like state which impairs myofilament sliding. Accordingly, we find that for contractions involving submaximal shortening velocities, muscle contraction power was significantly limited by decreased levels of MgATP level in the millimolar range. For a reduction of [MgATP] from 8 mM to 4 mM, maximum contraction power fell by 20%–25% (Table 1). Contractions that involve submaximal shortening speeds and high levels of mechanical power are relevant to the in vivo function of the heart to eject blood because myocardial contraction involves submaximal forces and velocities. Therefore, our finding of reduced mechanical power due to reduced MgATP level is likely relevant to systolic contraction of the heart in vivo. Decreased ATP levels in the failing heart could lead to decreased mechanical power and thus to decreased pump function. Indeed, the capacity to recruit mechanical power is suggested to serve as a unifying feature of heart failure (27). Finally, wall stress is increased in heart failure, which would require increased mechanical power. This increases the relevance to heart failure of our finding of a power deficit attributable to low MgATP level.

Mechanism for impaired myofilament contraction in low MgATP

Fig. 9 illustrates that while a computational model accounting for tension- and stain-dependent kinetics of cross-bridge cycling is able to effectively capture the shape of the observed force-velocity curve at a given [MgATP] concentration, the model does not capture the dependence of the curve on [MgATP] over the concentration range assessed here. This is because the model assumes an MgATP-myosin ATPase dissociation constant of $K_{MgATP} = 0.50$ mM. With this dissociation constant value, the model predicts apparent K_M values for maximal unloaded velocity and maximal isometric force in the range of 50–250 μM. These model predictions are consistent with the observations of Ebus et al. on maximal force (12) and Cooke and Bialek on maximal velocity (10). However, as a consequence of capturing reasonable ranges for the dependencies of maximal force and velocity on [MgATP], the model, as formulated, shows little dependence on [MgATP] over the range of 8–2 mM. Since it is generally understood that unbinding of myosin heads from the actin thin filament (cross-bridge detachment) is dependent on association of MgATP with the myosin ATPase, with an apparent dissociation constant of <250 μM, we do not expect a change in MgATP concentration from 8 to 4 mM to substantially affect the probability of detachment of a post-ratchet state cross-bridge.

Thus, there is an apparent incongruity between the submillimolar dependence of maximal force and velocity on [MgATP] and the substantial decrease in maximal power that is observed when decreasing [MgATP] from 8 to 2 mM. The mismatch between the best-fit model and the force-velocity data illustrated in Fig. 9 demonstrates that mechanisms captured by the model are inadequate to explain the effects of MgATP concentration on muscle dynamics over the micromolar-to-millimolar concentration range. Because we are unable to find a parameter regime that is consistent with realistic behavior over this wide range of MgATP concentration, it may be that the detachment kinetics or strain dependence of the detachment kinetics, and how these vary with changes in [MgATP], are not being appropriately formulated with the current model. Another possible mechanism by which MgATP concentration may affect cross-bridge dynamics is through the transitions between the super-relaxed (SRX) and non-super-relaxed (non-SRX) states of the myosin heads. X-ray diffraction studies in skinned muscle and molecular modeling studies suggest that association of deoxy-ATP with myosin may affect the kinetics of transition between the SRX and non-SRX states, suggesting a novel mechanism by which MgATP binding may influence muscle dynamics and power generation (28,29). A mechanism whereby the lower MgATP concentrations are associated with a greater stabilization of the SRX state may also be consistent with the

observed effects of [MgATP] on force development kinetics. It remains to be determined how this or other alternative mechanisms can explain how decreasing [MgATP] decreases submaximal force at non-zero velocities while increasing maximal isometric force.

Limitations

The current studies used an in vitro preparation, which differs considerably from the heart contracting in vivo. For example, in vivo myofilament contraction may be affected by intracellular compartmentation of MgATP that is not reflected in the in vitro studies. Moreover, in vitro studies involved low temperature, lack of cell membranes, and removal of the cytosol. We used contractions that were maximally activated by calcium for several seconds, in contrast to the submaximal and phasic contractions of the heart. Due to the ease of isolation, only trabeculae from the right ventricle were studied. However, impaired systolic dysfunction in heart failure predominantly involves the left ventricle. Thus, it is possible that differences in the physiology of RV versus left ventricular (LV) myocardium (including lower power output of RV myocardium) could lessen the relevance of our findings for understanding LV failure. Female mice were not studied. Finally, to approximate heart failure, we only varied the MgATP level, whereas heart failure involves increased levels of ADP and inorganic phosphate (Pi), which exert complex and divergent effects on contraction. Increased ADP level increases contraction force but lowers shortening velocity (30). Increased Pi level reduces contraction force but increases shortening velocity and mechanical power during loaded contractions (31). Further study is needed to determine how these divergent effects combine under conditions resembling heart failure with simultaneous changes in levels of ATP, ADP, and Pi.

CONCLUSIONS

A 50% reduction of MgATP, to a level typical of that found in heart failure, caused a reduced capacity for myofilament power generation. This finding suggests that the low MgATP level found in heart failure leads to myofilament dysfunction and thereby contributes to pump dysfunction. This further suggests that therapies designed to increase energy availability (e.g., use of mitotropes) or to inhibit degradation of adenine nucleotides might be beneficial for improving contraction in heart failure.

APPENDIX A: MATHEMATICAL MODEL OF MUSCLE DYNAMICS

Description of model

A cross-bridge dynamics model adapted from (5,21–23) and diagrammed in Fig. 9 *A* is used to simulate mechanics of the skinned-fiber preparation. The model is an explicitly spatially dependent model, where the attached states A_1, A_2, and A_3 are described by probability density functions $p_1(s,t)$, $p_2(s,t)$, and $p_3(s,t)$, and s is the strain, or deformation, associated with attached states. Ignoring the non-permissive (N) state, mysosin heads that are in the thick filament overlap zone may be in a permissive, or one of three attached states. The proportion of myosin heads that are permissible for binding to actin (associated with corresponding calcium-activated sites in the overlap zone) is denoted P, and p_1^0, p_2^0, and p_3^0 are the relative proportion of myosin heads that are in the attached states A_1, A_2, and A_3, as described below. Thus $P(t)$ can be calculated as

$$P(t) = 1 - p_1^0 - p_2^0 - p_3^0. \tag{A1}$$

The variables p_1^0, p_2^0, and p_3^0 are the zero$^{\text{th}}$ moments of the probability distributions, defined as

$$\begin{aligned} p_1^0(t) &= \int_{-\infty}^{+\infty} p_1(s,t)ds \\ p_2^0(t) &= \int_{-\infty}^{+\infty} p_2(s,t)ds \\ p_3^0(t) &= \int_{-\infty}^{+\infty} p_3(s,t)ds. \end{aligned} \tag{A2}$$

The strain distributions of attached states are governed by one-dimensional hyperbolic equations of Tewari et al. (22):

$$\begin{aligned} \frac{\partial p_1}{\partial t} + \frac{dL}{dt}\frac{\partial p_1}{\partial s} &= k_a\delta(s)U_{NR}P - \tilde{k}_d p_1 - \tilde{k}_1 e^{-\alpha_1 s}p_1 + k_{-1}e^{+\alpha_1 s}p_2 \\ \frac{\partial p_2}{\partial t} + \frac{dL}{dt}\frac{\partial p_2}{\partial s} &= \tilde{k}_1 e^{-\alpha_1 s}p_1 - k_{-1}e^{+\alpha_1 s}p_2 - k_2 e^{-\alpha_2 s}p_2 + \tilde{k}_{-2}p_3 \\ \frac{\partial p_3}{\partial t} + \frac{dL}{dt}\frac{\partial p_3}{\partial s} &= k_2 e^{-\alpha_2 s}p_2 - \tilde{k}_{-2}p_3 - \tilde{k}_3 e^{\alpha_3(s+s_3)^2}p_3. \end{aligned} \tag{A3}$$

The left-hand side of Eq. A3 is the material derivative defining how the velocity of sliding, dL/dt, influences the evolution of the strain distributions. The right-hand side defines the rate transitions from the permissive state to attached state A_1, from A_1 to A_2, from A_2 to A_3, and from A_3 back to the unattached state.

In the above equations the Tewari et al. model has been modified to include the factor $U_{NR}(t)$ in the attachment term $k_a\delta(s)U_{NR}P(t)$. This factor represents the proportion of myosin heads that are not in the super-relaxed state. The kinetics of super-relaxed/not-relaxed state transitions are described below.

The rate transitions in Eq. A3 are influenced by phosphate metabolite levels according to

$$\begin{aligned}
\tilde{k_d} &= k_d \frac{\frac{[Pi]}{K_{Pi}}}{1+\frac{[Pi]}{K_{Pi}}} \\
\tilde{k_1} &= k_1 \frac{1}{1+\frac{[Pi]}{K_{Pi}}} \\
\tilde{k_{-2}} &= k_{-2} \frac{\frac{[MgADP]}{K_{MgADP}}}{1+\frac{[MgADP]}{K_{MgADP}}+\frac{[MgATP]}{K_{MgATP}}} \\
\tilde{k_3} &= k_3 \frac{\frac{[MgATP]}{K_{MgATP}}}{1+\frac{[MgADP]}{K_{MgADP}}+\frac{[MgATP]}{K_{MgATP}}}
\end{aligned} \tag{A4}$$

as described by Tewari et al., where K_{Pi}, K_{MgADP}, and K_{MgATP} are the dissociation constants for inorganic phosphate, MgADP, and MgATP.

Unattached myosin heads are assumed to exist in either a super-relaxed (SR) or not super-relaxed (NR) state, as illustrated in Fig. 9 *A*. The fractions of unattached myosin heads in the SR and NR states are denoted U_{SR} and U_{NR}.

Transitions between the SR and NR states are governed by

$$\begin{aligned}
\frac{dU_{NR}}{dt} &= k_{SR} exp(\sigma_{XB}/\sigma_0) U_{SR} - k_{-SR}\, U_{NR}\, P \\
U_{SR} + U_{NR} &= 1.
\end{aligned} \tag{A5}$$

In the Campbell et al. (23) model the rate of transition from the SR to NR state is linearly dependent on active muscle tension, while here we assume that transition from SR to NR state is exponentially dependent on muscle tension, where σ_{XB} is the active cross-bridge contribution to tension. Only unattached (*P* state) myosin heads in the NR state are able to transition to the SR state.

Active and passive forces

The force associated with cross-bridges is computed from contributions from pre- and post-ratcheted states:

$$\sigma_{XB}(t) = k_{stiff,1}\left(p_2^1 + p_3^1\right) + k_{stiff,2}\,\Delta r\, p_3^0, \tag{A6}$$

where $k_{stiff,1}$ and $k_{stiff,2}$ are stiffness constants, Δr is the cross-bridge strain associated with ratcheting deformation, and $p_i^n(t) = \int_{-\infty}^{+\infty} s^n p_i(s,t) ds$.

Numerical approach

Eqs. A1, A2, A3, A4, A5, and A6 are numerically simulated by discretizing s and the probability densities $p_1(s,t)$, $p_2(s,t)$, and $p_3(s,t)$ on a one-dimensional grid. To simulate Eq. A3 we use an operator-splitting scheme that splits the advection step and the ODE-kinetic step into two separate steps. The model is implemented in MATLAB, and codes are available for download from https://github.com/beards-lab/Cardiac-Crossbridge-Explicit-Space-Discretization.

Parameter values and model behavior

Model parameter values are adjusted from those reported in Tewari et al. (22), Marzban and Beard (21), and Campbell et al. (23) to best match the force-velocity data obtained at [MgATP] = 2, 4, and 8 mM, as illustrated in Fig. 9 *B*. Estimated model parameters are listed in Table 2 (21).

To match the observed force-velocity data the cross-bridge cycle-rate constants (k_a, k_d, k_1, k_{-1}, k_2, k_{-2}, and k_3), the strain-dependency parameter α_3, the rate of transition to non-SRX state k_{SR}, the SRX transition force-dependency parameter σ_0, and the stiffness constants $k_{stiff,1}$ and $k_{stiff,2} \times \Delta r$ were adjusted to obtain the fit to the data in Fig. 9 *B*. (With parameter k_{-SR} is set to an arbitrarily large value the steady-state model behavior depends on the ratio k_{SR}/k_{-SR}, which is identified by adjusting k_{SR}.) With this relatively large number of adjustable parameters, no attempt is made to uniquely estimate their values. Rather, the set of parameter values reported in Table 2 demonstrates that the model is able to accurately capture the observed force-velocity relationship for [MgATP] = 8 mM, but not the differences observed for different MgATP concentrations. The model also reproduces the observed tension-redevelopment time constant of approximately 25–30 ms observed experimentally at [MgATP] = 8, but does not capture the dependence of the tension-redevelopment kinetics on [MgATP].

AUTHOR CONTRIBUTIONS

Designed research: D.A.B., K.S.C., P.M.L.J., N.C.C., and A.J.B.; performed research: A.J.B., B.M., O.Y.L., D.A.B., and K.S.C.; contributed analytic tools: D.A.B., B.M., and K.S.C.; analyzed data: A.J.B., B.M., D.A.B., and K.S.C.; wrote the paper: A.J.B., B.M., D.A.B., K.S.C., N.C.C., and P.M.L.J.

ACKNOWLEDGMENTS

This work was supported by Department of Veterans Affairs Merit Review Award I01BX000740 (A.J.B.) and National Heart, Lung, and Blood Institute grant R01 HL154624(A.J.B., D.A.B., N.C.C., P.M.L.J.).

DECLARATION OF INTERESTS

The authors declare no competing interests.

REFERENCES

1. Beer, M., T. Seyfarth, …, S. Neubauer. 2002. Absolute concentrations of high-energy phosphate metabolites in normal, hypertrophied, and failing human myocardium measured noninvasively with (31)P-SLOOP magnetic resonance spectroscopy. *J. Am. Coll. Cardiol.* 40:1267–1274.
2. Starling, R. C., D. F. Hammer, and R. A. Altschuld. 1998. Human myocardial ATP content and in vivo contractile function. *Mol. Cell. Biochem.* 180:171–177.
3. Yabe, T., K. Mitsunami, …, M. Kinoshita. 1995. Quantitative measurements of cardiac phosphorus metabolites in coronary artery disease by 31P magnetic resonance spectroscopy. *Circulation.* 92:15–23.
4. Stewart, L. C., R. Deslauriers, and V. V. Kupriyanov. 1994. Relationships between cytosolic [ATP], [ATP]/[ADP] and ionic fluxes in the perfused rat heart: a 31P, 23Na and 87Rb NMR study. *J. Mol. Cell. Cardiol.* 26:1377–1392.
5. Tewari, S. G., S. M. Bugenhagen, …, D. A. Beard. 2016. Influence of metabolic dysfunction on cardiac mechanics in decompensated hypertrophy and heart failure. *J. Mol. Cell. Cardiol.* 94:162–175.

6. Wu, F., J. Zhang, and D. A. Beard. 2009. Experimentally observed phenomena on cardiac energetics in heart failure emerge from simulations of cardiac metabolism. *Proc. Natl. Acad. Sci. USA.* 106:7143–7148.
7. Gao, X., D. G. Jakovljevic, and D. A. Beard. 2019. Cardiac metabolic limitations contribute to diminished performance of the heart in aging. *Biophys. J.* 117:2295–2302.
8. Neubauer, S. 2007. The failing heart–an engine out of fuel. *N. Engl. J. Med.* 356:1140–1151.
9. Takashi, R., and S. Putnam. 1979. A fluorimetric method for continuously assaying ATPase: application to small specimens of glycerol-extracted muscle fibers. *Anal. Biochem.* 92:375–382.
10. Cooke, R., and W. Bialek. 1979. Contraction of glycerinated muscle fibers as a function of the ATP concentration. *Biophys. J.* 28:241–258.
11. Pate, E., and R. Cooke. 1989. A model of crossbridge action: the effects of ATP, ADP and Pi. *J. Muscle Res. Cell Motil.* 10:181–196.
12. Ebus, J. P., Z. Papp, …, G. Stienen. 2001. Effects of MgATP on ATP utilization and force under normal and simulated ischaemic conditions in rat cardiac trabeculae. *Pflugers Arch.* 443:102–111.
13. Lopez, R., B. Marzban, …, D. A. Beard. 2020. Impaired myocardial energetics causes mechanical dysfunction in decompensated failing hearts. *Function (Oxf.).* 1:zqaa018.
14. Shimkunas, R., O. Makwana, …, M. B. Ratcliffe. 2014. Myofilament dysfunction contributes to impaired myocardial contraction in the infarct border zone. *Am. J. Physiol. Heart Circ. Physiol.* 307:H1150–H1158.
15. Fabiato, A., and F. Fabiato. 1979. Calculator programs for computing the composition of the solutions containing multiple metals and ligands used for experiments in skinned muscle cells. *J. Physiol. (Paris).* 75:463–505.
16. Kobirumaki-Shimozawa, F., K. Oyama, …, N. Fukuda. 2016. Nano-imaging of the beating mouse heart in vivo: importance of sarcomere dynamics, as opposed to sarcomere length per se, in the regulation of cardiac function. *J. Gen. Physiol.* 147:53–62.
17. Claflin, D. R., L. M. Larkin, …, J. A. Faulkner. 2011. Effects of high- and low-velocity resistance training on the contractile properties of skeletal muscle fibers from young and older humans. *J. Appl. Physiol. (1985).* 111:1021–1030.
18. Claflin, D. R., and J. A. Faulkner. 1989. The force-velocity relationship at high shortening velocities in the soleus muscle of the rat. *J. Physiol.* 411:627–637.
19. Hill, A. V. 1938. The heat of shortening and the dynamic constants of muscle. *Proc. R. Soc. Lond. Ser. B.* 126:136–195.
20. Giles, J., D. P. Fitzsimons, …, R. L. Moss. 2021. cMyBP-C phosphorylation modulates the time-dependent slowing of unloaded shortening in murine skinned myocardium. *J. Gen. Physiol.* 153
21. Marzban, B., R. Lopez, and D. A. Beard. 2020. Computational modeling of coupled energetics and mechanics in the rat ventricular myocardium. *Physiome*. https://doi.org/10.36903/physiome.12964970.
22. Tewari, S. G., S. M. Bugenhagen, …, D. A. Beard. 2016. Dynamics of cross-bridge cycling, ATP hydrolysis, force generation, and deformation in cardiac muscle. *J. Mol. Cell. Cardiol.* 96:11–25.
23. Campbell, K. S., P. M. L. Janssen, and S. G. Campbell. 2018. Force-dependent recruitment from the myosin off state contributes to length-dependent activation. *Biophys. J.* 115:543–553.
24. Edman, K. A., L. A. Mulieri, and B. Scubon-Mulieri. 1976. Non-hyperbolic force-velocity relationship in single muscle fibres. *Acta Physiol. Scand.* 98:143–156.
25. Woledge, R. C., N. A. Curtin, and E. Homsher. 1985. Energetic aspects of muscle contraction. *Monogr. Physiol. Soc.* 41:1–357.
26. Ogut, O., and F. V. Brozovich. 2003. Creatine phosphate consumption and the actomyosin crossbridge cycle in cardiac muscles. *Circ. Res.* 93:54–60.
27. Beard, D. A., S. L. Hummel, and F. Jezek. 2022. Heart failure as a limitation of cardiac power output. *Function (Oxf.).* 3:zqab066.
28. Ma, W., M. Childers, …, M. Regnier. 2020. Myosin dynamics during relaxation in mouse soleus muscle and modulation by 2′-deoxy-ATP. *J. Physiol.* 598:5165–5182.
29. Powers, J. D., C. C. Yuan, …, W. Ma. 2019. Cardiac myosin activation with 2-deoxy-ATP via increased electrostatic interactions with actin. *Proc. Natl. Acad. Sci. USA.* 116:11502–11507.
30. Cooke, R., and E. Pate. 1985. The effects of ADP and phosphate on the contraction of muscle fibers. *Biophys. J.* 48:789–798.
31. Hinken, A. C., and K. S. McDonald. 2004. Inorganic phosphate speeds loaded shortening in rat skinned cardiac myocytes. *Am. J. Physiol. Cell Physiol.* 287:C500–C507.